

Light-Induced Hypoxia-Triggered Living Nanocarriers for Synergistic Cancer Therapy

Wenliang Wang,^{†,§,||} Lin Lin,^{‡,||} Xiaojing Ma,^{*,†,ID} Bo Wang,[†] Sanrong Liu,[†] Xinxin Yan,^{†,§} Shengran Li,^{†,§} Huayu Tian,^{*,†,§,ID} and Xifei Yu^{*,†,§,ID}

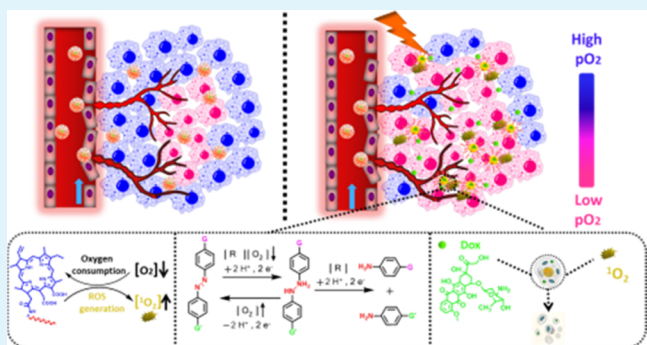
[†]Laboratory of Polymer Composites Engineering, Changchun Institute of Applied Chemistry and [‡]Key Laboratory of Polymer Ecomaterials, Changchun Institute of Applied Chemistry, Chinese Academy of Sciences, Changchun, Jilin 130022, P. R. China

^{*}University of Science and Technology of China, Hefei, Anhui 230026, P. R. China

Supporting Information

ABSTRACT: Living drug delivery system has been proposed as new concept materials because it is able to communicate with biological system, sense subtle changes in body microenvironment caused by disease, and then make rapid response to cure in the early stage of disease. Herein, taking full advantage of the tumor hypoxia physiology and successive effects of photodynamic therapy (PDT), we designed a new living delivery system via combining the PDT and hypoxia-responsive chemotherapy, abbreviated as Ce6-PEG-Azo-PCL. Then, according to the fact that oxygen can be converted into reactive oxygen species during irradiation of the photosensitizer, tumor cells could be killed after the poly(ethylene glycol) (PEG) conjugated photosensitizer chlorine e6 was irradiated at the tumor site. What is more, the continuous consumption of oxygen could further amplify the hypoxia condition of tumor and trigger the disassembly of hypoxia-responsive azobenzene bridges at the tumor site to release loaded therapeutics drugs doxorubicin. The ongoing collaboration with PDT and hypoxia-responsive chemotherapy provided an integrated therapeutic effect *in vitro* and *in vivo* to suppress tumor growth.

KEYWORDS: living biomaterials, hypoxia, light-induced, chlorine e6, synergistic therapy



1. INTRODUCTION

With further research and more clarity on tumor pathophysiology, various tactics have been developed to cure cancer, such as the photodynamic therapy (PDT),^{1–5} hypoxia-targeted treatment,^{7–10} and so on. However, the sluggish communication or inefficient interactive properties between the drug delivery systems and biological systems severely gap in the desired therapeutic efficacy and poor realities. Very recently, living drug delivery system, which is able to integrate and exchange information with biological systems and make rapid response to the subtle changes in the diseased body, has been proposed by Langer as the next-generation biomaterials,⁶ and their excellent properties of minimizing nonspecial toxicity and greatly enhancing the therapeutical efficacy have also been demonstrated by other groups.^{11–15} Thus, it is intriguing and imminent to build a “smart” living therapeutics that can sense and respond to the commands of tumor biological micro-environment in the body. This living system will not only target and kill the tumor cells at an early form and reduce the damage of normal tissues to the minimum, but also make it possible to stop the tumor reoccurrence and metastasis, which bring enormous prospect in curing cancer.

Hypoxia, which is caused by uncontrollable cell division and inadequate blood supply, is a striking feature of malignant tumor contrast to normal tissues.^{16–19} Of note, hypoxia-activated systems, such as polymersomes,⁹ polymer nanoparticles,^{8,10} upconverting nanoparticles,³ and molecular imaging probe,²⁰ have been developed to target, detect, and fight against hypoxic tumor. However, they cannot do work unless the oxygen deficiency reach a certain extent, and the slight decrease in oxygen pressure in tumor cells relative to other normal cells inevitably hindered their therapeutic efficacy.^{7,21,22} Interestingly, the intracellular low-oxygen micro-environment was generated as the appurtenance in photodynamic therapy, where the oxygen in the tumor cells was continuously consumed through the photosensitizer (such as chlorine e6) upon the irradiation of laser to produce reactive oxygen species (ROS).^{23–25} It provides a perspective to enhance cancer therapy via integrating the hypoxia-activated system into PDT.

Received: March 1, 2018

Accepted: May 21, 2018

Published: May 21, 2018



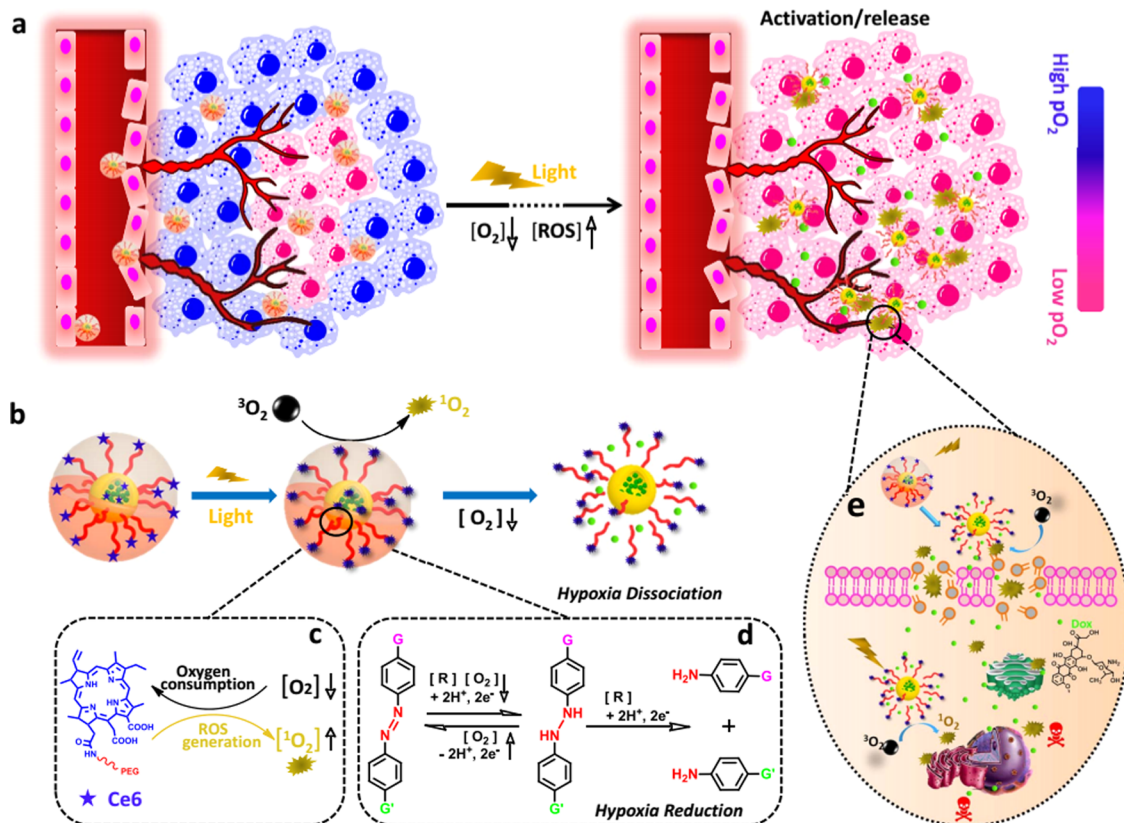


Figure 1. (a) Schematic of how the light-activated Dox@NP nanoparticles worked in combination with hypoxia-triggered and PDT treatment strategy. (b) Generation of the ROS and hypoxia-induced disassembly upon laser irradiation. The mechanism of (c) photosensitized reaction induced by Ce6 and (d) stepwise reduction of azobenzene in hypoxia environment.⁹ (e) Light-driven synergistic therapy of ROS and Dox-based chemotherapy.

In this report, we developed a kind of “one stone second birds” living drug delivery system to improve the anticancer therapeutic efficacy in cervical cancer. This living drug delivery system, abbreviated as Ce6-PEG-Azo-PCL and shown in Figures 1a and S1, was made up of three primary constituents: the hypoxia-induced cleaved azobenzene (Azo) bridges to sense hypoxia microenvironment, the biodegradable hydrophobic poly(ϵ -caprolactone) (PCL) as a hydrophobic segment, and hydrophilic poly(ethylene glycol) (PEG)-decorated photosensitizer chlorine e6 (Ce6) to enhance loading content and minimize premature release of Ce6. Doxorubicin (Dox), a vigorous anticancer drug approved by FDA, can effectively suppress tumor growth by inserting into minor grooves of DNA to inhibit their replication and transcription and^{26–29} was integrated into this functional nanocarrier subsequently. After intravenous injection, the Ce6-PEG-Azo-PCL@Dox (Dox@NP) nanocarriers could accumulate in the tumor via enhanced permeability and retention (EPR) effect.^{30,31} With subsequent cellular internalization, programmed successive triggers would activate spontaneously and synergistically upon irradiation. (1) As shown in Figure 1b,c, photosensitizer Ce6 was activated to generate ROS and hypoxia microenvironment after irradiation.^{5,32,33} (2) Hypoxia responsive azobenzene was triggered to reduce stepwise by reductases to aniline derivatives under the oxygen-deficient environment (Figure 1d) after activation of primary trigger,^{8,9,34,35} and further triggered the release of anticancer drugs at tumor site. (3) The tumor cells apoptosis was subsequently triggered in the presence of ROS and chemotherapeutic drug Dox. The ongoing collaboration with

PDT and hypoxia-triggered chemotherapy (Figure 1e) provided an integrated therapeutic effect to suppress tumor growth.

2. EXPERIMENTAL SECTION

2.1. Materials. Polymer *N*-*tert*-butoxycarbonyl-PEG₃₄₀₀-amine (*N*-Boc-PEG₃₄₀₀-NH₂) was supplied from Ponsure Bio, Inc. (China, Shanghai). The chemicals of azobenzene-4,4'-dicarboxylic acid, 2-(2-aminoethoxy)ethanol, ϵ -caprolactone, *N*-hydroxysuccinimide (NHS), 1,3-diisopropylcarbodiimide (DIC), and tin(II) 2-ethylhexanoate (Sn(Oct)₂) were purchased from Aladdin. Chlorine e6 (Ce6), doxorubicin hydrochloride (Dox-HCl), and trifluoroacetic acid were purchased from Sigma-Aldrich. All of the chemicals were used as obtained unless otherwise mentioned.

2.2. Reaction of *N*-Boc-PEG₃₄₀₀-NH₂ with Azobenzene-4,4'-dicarboxylic Acid. Azobenzene-4,4'-dicarboxylic acid was conjugated to *N*-Boc-PEG₃₄₀₀-NH₂ by previous method.^{8,9} Briefly, azobenzene-4,4'-dicarboxylic acid (0.27 g, 1 mmol), NHS (28 mg, 0.25 mmol), and DIC (31.5 mg, 0.25 mmol) were dissolved in pyridine (10 mL) with stirring at room temperature and then the mixed solution of *N*-Boc-PEG₃₄₀₀-NH₂ (0.68 g, 0.2 mmol) and pyridine (5 mL) was added dropwise. The solution was continuously stirred for 24 h under the Ar atmosphere at room temperature. After that, the solid was filtered off and the filtrate was added dropwise into excessive methanol to precipitate unreacted azobenzene-4,4'-dicarboxylic acid. The supernatant was concentrated under rotary evaporation and the product collected and dried under vacuum with orange color (0.6 g, yield: 81.7%). ¹H NMR (400 MHz, CDCl₃): δ (ppm) 8.21–8.23 (d, Ar-H-CONH), 7.95–8.03 (m, Ar-H-N=N-), 3.30–3.93 (m, -OCH₂CH₂O-), 1.44 (s, -COOC(CH₃)₃).

2.3. Reaction of *N*-Boc-PEG₃₄₀₀-Diphenylazacarboxylate with 2-(2-Aminoethoxy)ethanol. Briefly, *N*-Boc-PEG₃₄₀₀-diphenylazacar-

boxylate (0.58 g, 0.17 mmol), NHS (57.5 mg, 0.5 mmol), and DIC (63 mg, 0.5 mmol) were dissolved in dimethyl sulfoxide (DMSO) (10 mL) at room temperature with continuous stirring and then 2-(2-aminoethoxy)ethanol (44.5 mg, 0.5 mmol) was added. After reacting for 24 h, the resulting solution was dialyzed (MWCO 1000) for 24 h and then lyophilized with the final product (0.56 g, yield: 96.5%). ¹H NMR (400 MHz, CDCl₃): δ (ppm) 8.20–8.25 (d, Ar-H-CONH), 7.93–8.01 (m, Ar-H-N=N-), 3.25–3.89 (m, -OCH₂CH₂O-), 1.44 (s, -COOC(CH₃)₃).

2.4. Synthesis of the Block Copolymer *N*-Boc-PEG₃₄₀₀-Diphenylazacarboxylate-Poly(ϵ -caprolactone) (*N*-Boc-PEG₃₄₀₀-Azo-PCL). The product obtained from the previous step (0.51 g, 0.15 mmol), ϵ -caprolactone (0.855 g, 7.5 mmol), and Sn(Oct)₂ (0.15 g, 0.37 mmol) were added into a flask with 15 mL anhydrous toluene. Then, the mixed solution was reacted at 110 °C with continuous stirring for 5 h. After that, the solution was added dropwise into excessively cold diethyl ether to precipitate the product. After precipitating for three times, the precipitate was obtained and dried under vacuum for 24 h (1.10 g, yield: 80.5%). ¹H NMR (400 MHz, CDCl₃): δ (ppm) 8.19–8.23 (d, Ar-H-CONH), 7.91–8.03 (m, Ar-H-N=N-), 4.05 (t, -CH₂COO-), 3.25–3.89 (m, -OCH₂CH₂O-), 2.30 (t, -O-CH₂-CH₂-), 1.63 (m, -OCH₂-CH₂-CH₂-CH₂-COO-), 1.44 (s, -COOC(CH₃)₃), 1.38 (m, -OCH₂-CH₂-CH₂-CH₂-COO-).

2.5. Reaction of the *N*-Boc-PEG₃₄₀₀-Azo-PCL with Chlorine e6 (Ce6). First, polymer *N*-Boc-PEG₃₄₀₀-Azo-PCL (0.5 g) was dissolved in 5 mL CH₂Cl₂ containing 0.8 mL trifluoroacetic acid. After reacting for 4 h at room temperature, the mixture was added dropwise into excessive diethyl ether. After precipitating for three times, the precipitate was collected and dried under vacuum. ¹H NMR (400 MHz, CDCl₃): δ (ppm) 8.19–8.23 (d, Ar-H-CONH), 7.91–8.03 (m, Ar-H-N=N-), 4.05 (t, -CH₂COO-), 3.25–3.89 (m, -OCH₂CH₂O-), 2.30 (t, -O-CH₂-CH₂-), 1.63 (m, -OCH₂-CH₂-CH₂-CH₂-COO-), 1.38 (m, -OCH₂-CH₂-CH₂-CH₂-COO-). The peak at chemical shift 1.44 disappeared, indicating that *N*-tert-butoxycarbonyl group was totally removed.

Then, the product obtained from the previous step (0.4 g, 0.045 mmol), NHS (17.25 mg, 0.15 mmol), DIC (18.9 mg, 0.15 mmol), and chlorine e6 (30 mg, 0.05 mmol) were dissolved in DMSO (10 mL) at room temperature with continuous stirring. After 24 h in dark, the mixture was added dropwise into 100 mL deionized water with continuous stirring and then dialyzed (MWCO 14 000) for 48 h to remove unreacted Ce6. The final product was obtained with lyophilization (0.41 g, 95.3%), wherein the conjugation randomly occurred with one of the carboxyl groups in Ce6. ¹H NMR (400 MHz, CDCl₃): δ (ppm) 8.75–9.73 (m, Ce6-H-), 8.19–8.23 (d, Ar-H-CONH), 7.91–8.03 (m, Ar-H-N=N-), 4.05 (t, -CH₂COO-), 3.25–3.89 (m, -OCH₂CH₂O-), 2.30 (t, -O-CH₂-CH₂-), 1.63 (m, -OCH₂-CH₂-CH₂-CH₂-COO-), 1.38 (m, -OCH₂-CH₂-CH₂-CH₂-COO-).

2.6. Preparation and Characterization of Dox/Hypoxia-NP. For the preparation of Dox-loading nanoparticles, polymer Ce6-PEG-Azo-PCL (15 mg) and Dox-HCl (4 mg) were dissolved in DMSO (3 mL) and then trimethylamine (60 μ L) was added and stirred for 1 h. After that, the solution was added dropwise into 10 mL deionized water with rapid stirring. After stirring for 3 h, the solution was dialyzed against deionized water (1 L) for 1 day to remove free Dox and solvent, wherein the deionized water was refreshed every 12 h. In addition, 2 mL solution was extracted and lyophilized to measure the drug-loading content and drug-loading efficiency. The size distribution and morphology of Dox/NP were determined by the Zetasizer (Nano-ZS) and transmission electron microscope (TEM) (JEOL JEM-1011). The ultraviolet-vis (UV-vis) spectra were determined via NanoDrop 2000c. The amount of Dox and Ce6 were measured by the UV-vis spectrum at 488 nm of Dox and 650 nm of Ce6.

2.7. Determination of ROS in Vitro. 1,3-Diphenylisobenzofuran (DPBF) was used as the ROS probe. In brief, DPBF, which dissolved in ethanol (10 μ L, 1.35 mg/mL), was added into the solution of free Ce6 and NP (3 mL, 120 μ g/mL). The mixture was then irradiated with 671 nm light for the designated time. After that, the absorption

spectra of mixture were determined on UV-vis spectrophotometer (NanoDrop 2000c) at fixed time. The ROS quantum yields of free Ce6 and NP in the solution were measured according to the absorption intensity at 408 nm.

2.8. Intracellular Oxygen Consumption Assay and ROS Generation Detection. ROS/ID^R hypoxia/oxidative stress detection kit (Enzo Life Sciences) was used to determine the oxygen consumption and the generation of ROS inside the cells. The HeLa cells were incubated in confocal dish with 70% confluence. The sufficient volume of hypoxia/oxidative stress detection mixture that contains either the NP (the concentration of Ce6 was 3 μ g/mL), hypoxia inducer control (deferoxamine, DFO), or ROS inducer control (pyocyanin, Pyo) at desirable working concentration was added. After incubating for desirable time (2 h for NP, 3.5 h for hypoxia inducer control, and 0.5 h for ROS inducer control) in dark, the NP-treated HeLa cells were exposed to the 671 nm laser irradiation at 10 mW for 5 min, or incubated for same time in dark. After that, the HeLa cells were washed with phosphate-buffered saline (PBS) for three times and confocal laser scanning microscope (CLSM, LSM 700 Carl Zeiss Microscopy) was used to capture the image. The ROS detection requires a filter set compatible with fluorescein (Ex/Em: 490/525 nm) and the hypoxia detection filter set with Texas Red (Ex/Em: 596/670 nm).

What is more, the flow cytometry was also used to study the oxygen consumption and ROS generation inside the cells by BD Accuri C6 Plus Flow Cytometry (BD Biosciences). The HeLa cells were treated and detected according to the product manual. Of note, the fluorescence signal of ROS detection reagent was measured using FL1 channel and the hypoxia detection reagent using FL3 channel, no compensation correction is required.

2.9. In Vitro Drug Release. The drug release from the nanoparticles was measured via dialysis against phosphate buffered saline with or without 671 nm laser irradiation. Dox-loaded NP (2 mL) solution containing rat liver microsomes (20 μ L, 20 mg/mL) (Shanghai Bioroot Biological Technology Co., Ltd, China) and nicotinamide adenine dinucleotide phosphate disodium salt (NADPH) (100 μ M) were exposed to 671 nm laser irradiation at 10 mW for 5 min or in dark. Then, the solution was added into the dialysis bag (MWCO 3500) and immersed in a tube containing 18 mL PBS with continuous stirring at 37 °C. At the desirable incubation time, the dialysis solution (1 mL) outside the dialysis bag was taken out and determined via UV-vis spectrophotometer (NanoDrop 2000c) at 488 nm. Fresh medium with the same volume was replaced after detection.

2.10. Intracellular Drug Trafficking. To evaluate the hypoxia-triggered intracellular drug release, the HeLa cells were seeded in confocal dish with 70% confluence. Then, the cells were treated with Dox-loaded NP (with the concentration of Dox 10 μ g/mL). After incubation for 1 h, the cells were washed twice with PBS and fresh Dulbecco's modified Eagle's medium (DMEM) was replaced. Then, the cells were exposed to 671 nm laser irradiation at 10 mW for 5 min. After incubation for desirable time, the cells were washed three times with PBS and fixed with 4% formaldehyde for 15 min and stained with 4',6-diamidino-2-phenylindole (10 μ g/mL) for 10 min. Confocal laser scanning microscope (CLSM, LSM 700 Carl Zeiss Microscopy) was used to image (Ex/Em: 488/575 nm). As control, the HeLa cells were treated in the same condition except without laser irradiation or with laser irradiation in the presence of ROS scavenger vitamin C (200 μ g/mL).

2.11. Cell Viability Assay. The cytotoxicity of Dox-loaded NP toward HeLa cells was evaluated by Celltiter-Blue assay. The HeLa cells were seeded in 96-well plates at a density of 1×10^4 cells/well and incubated for 24 h. Then, the medium was replaced by fresh DMEM containing different concentration of free Dox, NP, and Dox-loaded NP. After incubation for 4 h, the cells were exposed to 671 nm laser irradiation for 5 min at the power of 10 mW or in dark. The cells were incubated for another 24 h and then Celltiter-Blue reagent (10 μ L/well) was added and the plates were incubated for another 4 h. Finally, the fluorescence intensity was measured by microplate reader (Ex/Em: 560/590 nm).

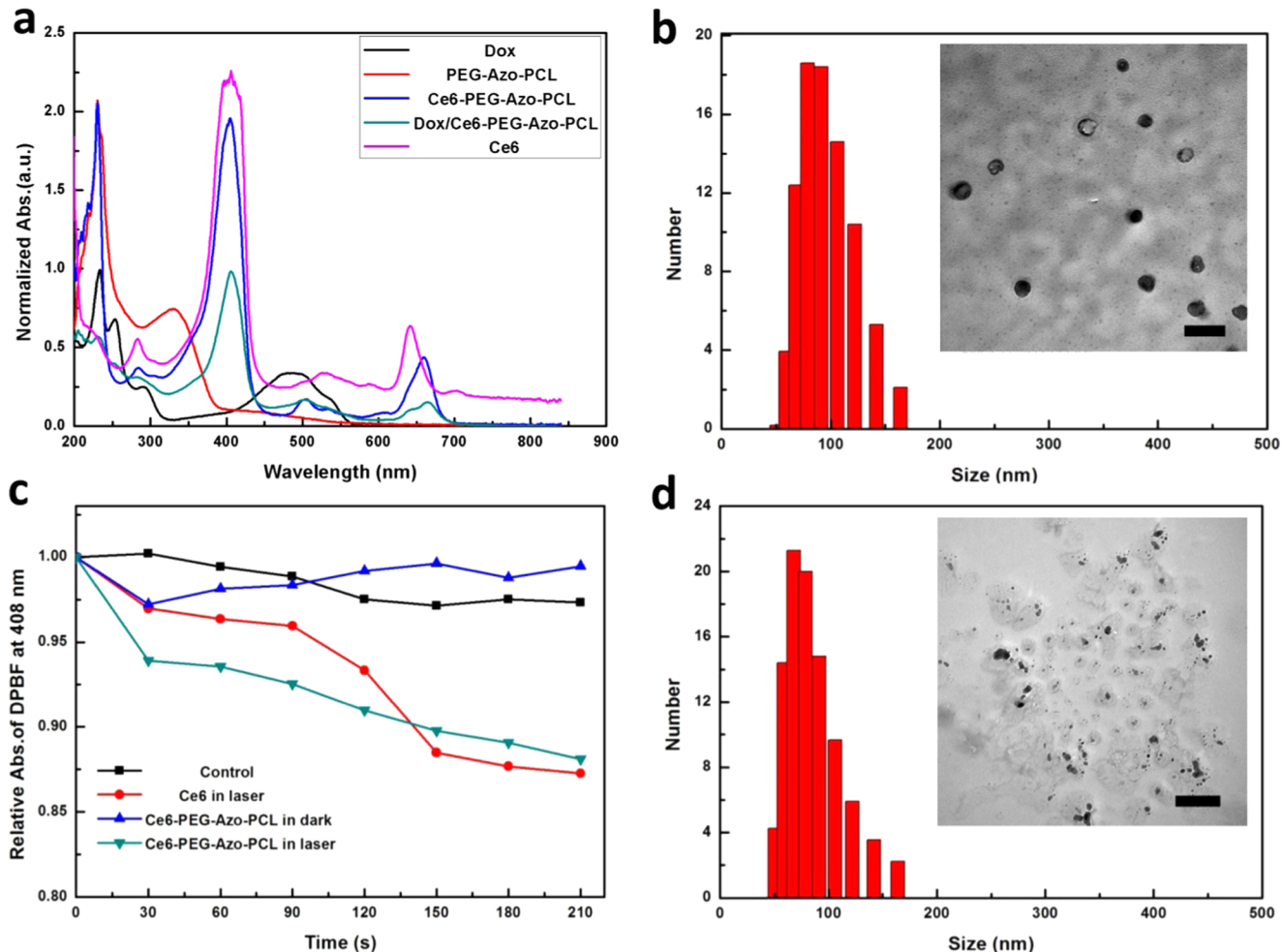


Figure 2. (a) UV-vis spectra of various substances in water. The size distributions of Ce6-PEG-Azo-PCL (NP) nanoparticles before (b) and after (d) laser irradiation. The insets are TEM images of NP nanoparticles before and after laser irradiation. Scale bar: 200 nm. (c) Relative UV-vis absorption intensities of DPBF at 407 nm in water after laser irradiation for desirable time interval.

2.12. Animals and Tumor Model. Male Balb/c mice, 4–6 weeks old, and nude mice (21 ± 2 g) from Vital River Company (Beijing, China) were used. All of the animal procedures were in accordance with the Animal Care and Use Committee of Northeast Normal University. HeLa tumor was established by subcutaneous injection of 1×10^7 HeLa cells into the desirable position and the tumor volume was determined via the following equation: volume = $0.5 \times a \times b^2$, where a and b were represented for length and width, respectively. The length and width of the tumor were measured via Vernier caliper.

2.13. In Vivo Imaging Detection. For real-time dynamic gauging of the accumulation of various Dox formulations at the tumor site, in vivo imaging was conducted via Maestro In Vivo Imaging System (Cambridge Research & Instrumentation, Inc.). Free Dox, Ce6-PEG-Azo-PCL@Dox (Dox@NP), was injected into the HeLa tumor bearing nude mice via tail vein at Dox-equivalent dose of 3 mg/kg body weight when the tumor volume reached 100–300 mm³. The near-infrared (NIR) fluorescence imaging was conducted at 3, 6, 12, and 24 h after injection. After 24 h, the mice were sacrificed and the tumor and various organs (heart, liver, spleen, lung, and kidney) were excised and prepared for NIR fluorescence imaging.

2.14. In Vivo Antitumor Efficacy. The HeLa tumor-bearing mice were randomly divided into six groups and treated with different formulations: (1) saline; (2) laser only; (3) Dox (3 mg/kg) with laser; (4) Ce6-PEG-Azo-PCL (Ce6 of 2.3 mg/kg) with laser; (5) Ce6-PEG-Azo-PCL@Dox (Ce6 of 2.3 mg/kg, Dox of 3 mg/kg); (6) Ce6-PEG-Azo-PCL@Dox (Ce6 of 2.3 mg/kg, Dox of 3 mg/kg) with laser. At 6 h after injection, groups 2, 3, 4, and 6 were treated via irradiating the tumor region with 671 nm laser at the power of 150 mW for 10 min.

The body weight and tumor volume were measured every other day. The treatment efficacy was evaluated by monitoring the relative changes of tumor volume and body weight. After 15 days, all of the mice were sacrificed, and the tumors and major organs (heart, liver, spleen, lung, and kidney) were excised to fix in 10% neutral buffered formalin and stained via hematoxylin and eosin (H&E) for pathological analysis.

2.15. Statistics. All of the measurements presented are expressed as mean \pm standard deviation (S.D.). Student's *t*-test was used to compare the statistical significance (**P* < 0.05, ***P* < 0.01, ****P* < 0.001).

3. RESULTS AND DISCUSSION

To confirm our design, we first synthesized azobenzene functional primary Boc-protected hydroxyl-terminated poly(ethylene glycol) (*N*-Boc-PEG₃₄₀₀-OH) macroinitiator, and the details are shown in Figure S1. The complete reaction was demonstrated via the integration ratio between the protons of *N*-*tert*-butoxycarbonyl and methylene protons of azobenzene (Figures S2 and S3), and the UV-vis spectra showed a remarkable absorption peak at 330 nm for azobenzene groups (Figure 2a). Next, the *N*-Boc-PEG₃₄₀₀-diphenylazacarboxylate-poly(*ε*-caprolactone) copolymers were synthesized via ring-opening reaction in the appearance of previous macroinitiator, whose structure and polymerization degree were confirmed by NMR analyses and gel permeation chromatography (GPC)

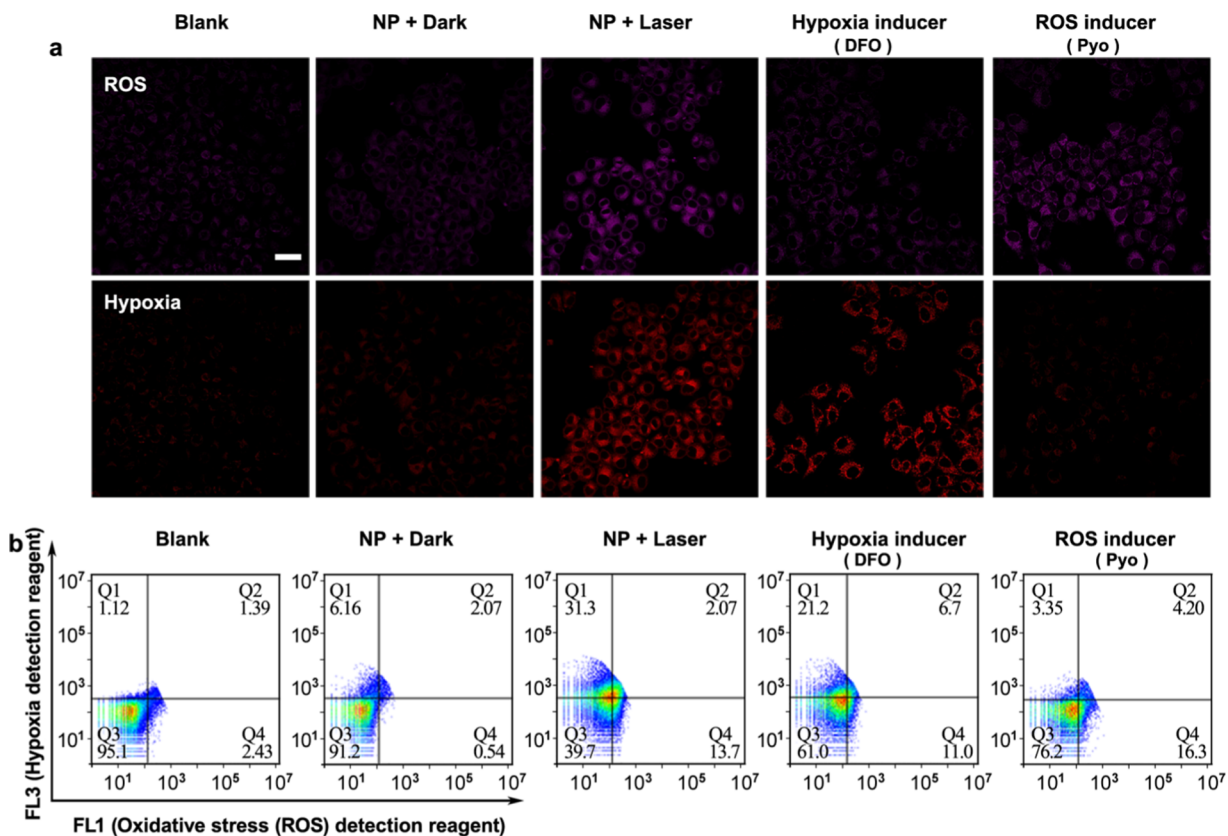


Figure 3. (a) Confocal images of HeLa cells treated with NP and ROS/hypoxia detection fluorescence probes in dark or laser irradiation. Scale bar: 20 μ m. (b) Flow cytometry analysis of intracellular generation of ROS and hypoxia in HeLa cells with or without laser irradiation.

tests (Figures S4 and S6, Table S1), indicating a good controllability of polymerization and a low polydispersity. Then, trifluoroacetic acid was added to remove the Boc groups to generate terminated amine groups, and Ce6 molecules were conjugated to the polymer chain via moderate amidation reaction (Figure S5). According to the UV-vis results, the characteristic absorption band at 610–690 nm was remarkable, which was attributed to the conjugated Ce6 (Figure 2a). Based on the UV-vis absorption intensity in 650 nm, approximately 7.2 wt % of Ce6 was conjugated to the chain.

Then, we used nanoprecipitation method³¹ to prepare the Ce6-PEG-Azo-PCL (NP) and Dox-loaded Ce6-PEG-Azo-PCL (Dox@NP) nanoparticles. The morphology and size distribution were determined by TEM and dynamic light scattering (DLS), as shown in Figure 2b. It can be found that these nanoparticles stably exist in the form of individual spherical morphology with the desirable size around 100 nm and narrow size distribution (<0.25). The ζ potential of the NP was measured to be -23.6 ± 0.4 mV, which was attributed to the redundant carboxyl groups in Ce6 (Figure S7a). It is interesting to find that there is only little increase in the particle size (Figure S7b) after encapsulation of Dox. What is more, SPSS software was applied to calculate the average diameter and make statistics of micelles distribution. As shown in Figures S8 and S9, the diameter of these micelles was about 73.66 ± 26.15 nm. After loading Dox, the size was increased to be about 90.69 ± 36.23 nm. The DLS gives the hydrodynamic diameter, which includes the core and the swollen corona of micelles, whereas TEM only confirms the core of micelles in the dried state. Thus, the diameter measured via TEM was smaller than the hydrodynamic diameter obtained by DLS, which was consistent

with other's works.^{26,30,31} Meanwhile, according to the UV-vis spectra detection of Dox in 488 nm, the drug-loading content and drug-loading efficacy with Dox were calculated to be about 9.3 wt % and 79.1%, respectively.

The ROS generation of NP induced by the conjugated Ce6 upon laser irradiation was detected using 1,3-diphenylisobenzofuran (DPBF) as the indicator, whose absorption in 408 nm could be irreversibly quenched by the generation of $^1\text{O}_2$.^{36–38} It can be found from Figure 2c that the absorption intensity of DPBF in the NP solution was reduced by 11.9% after the 671 nm laser irradiated for 210 s and by 12.8% for free Ce6 solution under the same condition. However, there are no obvious absorption changes in NP and free Ce6 solution in dark, suggesting the ROS could be effectively produced under laser irradiation.

Impressively, the TEM images showed that the previous uniform nanoparticles showed irregular morphology after irradiation for 5 min and the average dynamic diameter, measured by DLS, decreased to 75.0 ± 3.6 nm (Figure 2d), further indicating the disassembly of these nanoparticles. The most important thing is that as the accessory of PDT, the hypoxia microenvironment was inevitably and automatically created because the oxygen has been continuously consumed during irradiation, and the azobenzene bridges would undergo a series of successive reductions (main mechanism shown in Figure 1d)^{9,34,35,39} under the reducing hypoxic microenvironment, which disrupted the integrality of the nanoparticles' spherical morphology. What is more, as the azobenzene linker can convert into the anilines at the hypoxic reduction condition, the ζ potential of the NP was increased to -19.1 ± 1.0 mV (Figure S6c). These data directly or indirectly

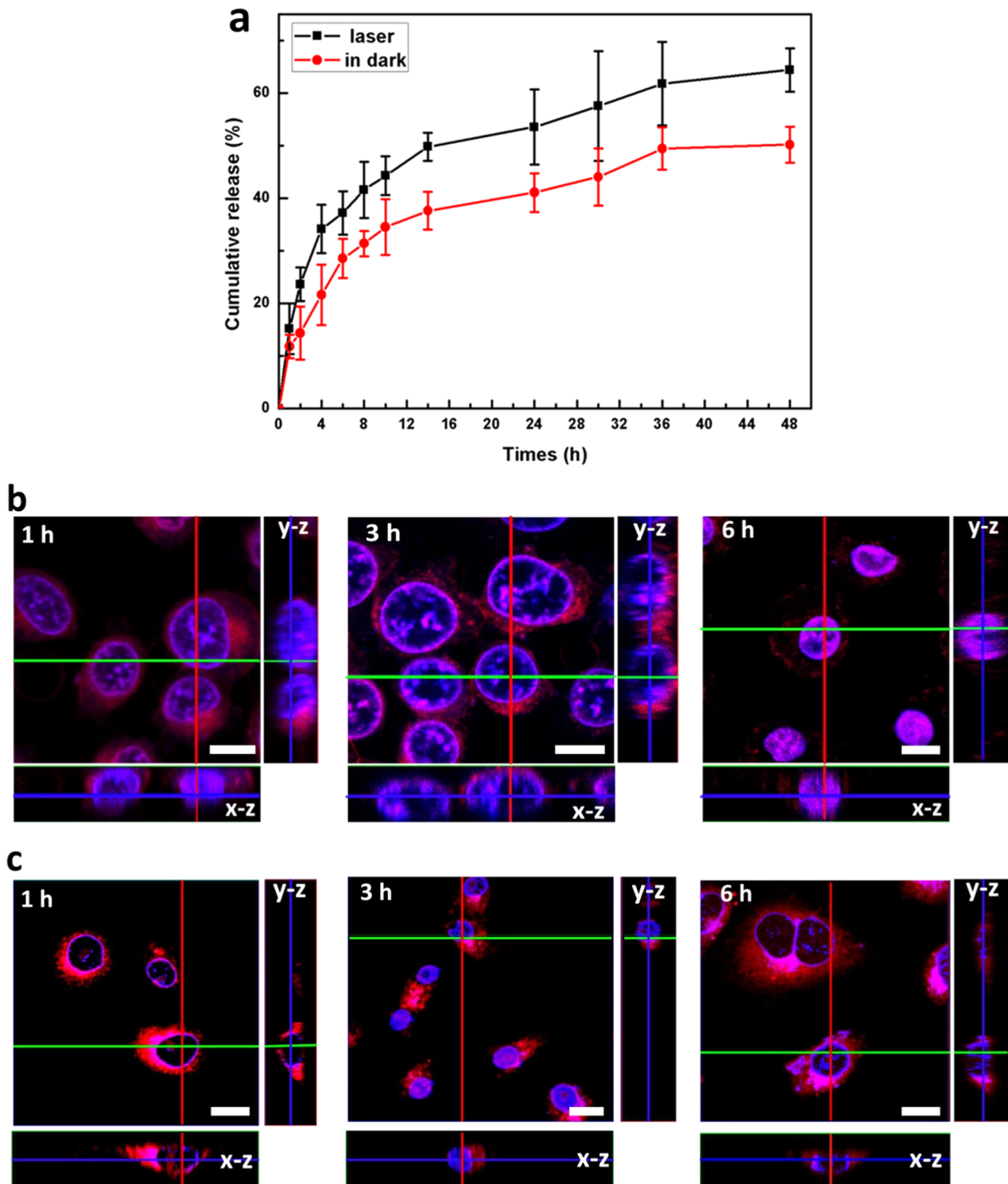


Figure 4. (a) In vitro Dox release from Dox@NP in PBS with or without laser irradiation. (b) Z-Stack confocal images of HeLa cells treated with Dox@NP under laser irradiation (c) and in dark, and observed after further incubation for 1, 3, and 6 h. Scale bar: 10 μ m.

demonstrated that these NP nanoparticles could effectively generate ROS and hypoxia microenvironment during laser irradiation, and suggested they had great potential to be used as a living nanocarrier with light-induced hypoxia-triggered characteristics.

We also directly evaluated the intracellular hypoxia/ROS generation mediated by NP with the help of flow cytometry and confocal laser scanning microscopy (CLSM). The HeLa

cells were incubated with NP with or without laser irradiation, and the hypoxia/ROS fluorescence probes were added. The blank cells were set as negative control, and the cells incubated with ROS inducer (pyocyanin, Pyo) or hypoxia inducer (deferoxamine, DFO) were set as positive controls, respectively. Interestingly, after irradiation for 5 min, the remarkable magenta (indicator of ROS) and red (indicator of hypoxia) fluorescence signals were observed in the NP-treated cells, but

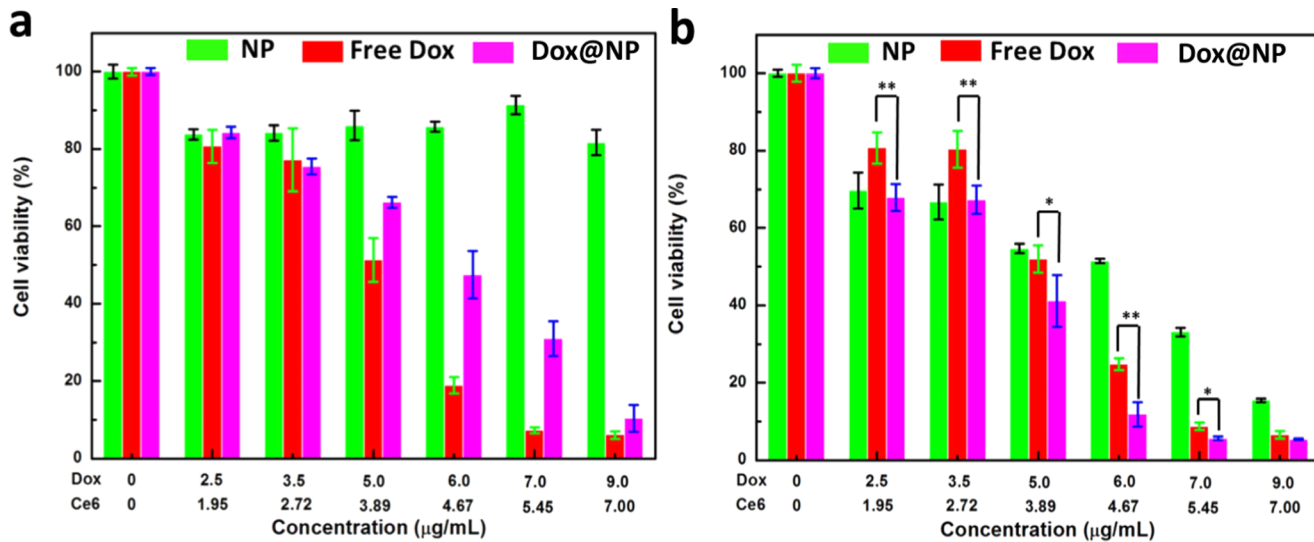


Figure 5. In vitro cytostatic effects of Dox, NP, and Dox@NP against HeLa cells after incubation for 24 h with or without laser irradiation, (a) incubation in dark, and (b) laser irradiation for 5 min. *P < 0.05, **P < 0.01, ***P < 0.001.

only weak fluorescence signal can be observed in those NP-incubated cells without irradiation (Figure 3a), which indicated the effective light-induced generation of ROS and hypoxia inside the tumor cells upon irradiation. Furthermore, we also quantified the intracellular production of ROS and hypoxia using flow cytometry. As shown in Figure 3b, the intracellular ROS and hypoxia ratios were increased to 28.9 and 46.5% after irradiation, whereas no changes were observed in the cells without laser irradiation.

In addition, the hypoxia-triggered drug release manner induced by light was also evaluated. Herein, the Dox release in vitro was determined through the dialysis method^{27–29} with or without laser irradiation. The Dox@NP solution at reducing condition was exposed to 671 nm laser for 30 min at the power of 10 mW before transferring into dialysis bags. After dialysis for 48 h, about 69.2% Dox was released at the reducing condition containing nicotinamide adenine dinucleotide phosphate disodium salt (NADPH) and rat liver microsomes, whereas only 49.7% of Dox was released in the same condition when without irradiation (Figure 4a), suggesting that the Dox release behavior was light triggered.

It is widely known that the anticancer drug Dox exerts its cytostatic effects by inhibiting the DNA in nucleus. Therefore, it is crucial whether Dox could be effectively released into the nucleus after Dox@NP entered into the cells. Here, the intracellular Dox release was determined using Z-stack confocal laser scanning microscopy (CLSM) imaging.⁴⁰ The HeLa cells were treated by Dox@NP solution under laser irradiation at the power of 10 mW for 5 min and then the intracellular Dox location was observed at the desirable time. The Z-stack confocal images and two-dimensional confocal images revealed that the Dox was effectively released into the nucleus with passing of time, and nearly all of the Dox was released into the nucleus after further incubation for 6 h (Figures 4b and S10). Comparatively, almost no Dox was observed around the nucleus even after 6 h of incubation in dark condition (Figures 4c and S11). Meanwhile, the drug release manner was remarkably hindered by the presence of ROS-scavenging inhibitor vitamin C, and only small amount of Dox could be released into the nucleus (Figures S12 and S13) after further 6 h incubation. This suggested that this living nanocarrier has a

significant synergistic effect on intracellular drug release, which was mainly attributed to the light-induced generation of ROS and collateral damage of the lysosomal/endosomal membrane.^{21,41} Otherwise, the continuous intracellular oxygen consumption produced the local hypoxia microenvironment, which triggered the disassembly of Dox@NP and further facilitated the Dox accumulation in nucleus. Collectively, all of the results demonstrated that the Dox could be effectively released to the nucleus to exert their cytostatic effects under laser irradiation.

Next, we evaluated the in vitro cytostatic effects of Dox@NP against the HeLa cells by Celltiter-Blue assay. As shown in Figure 5a,b, the cytostatic effect of free Dox was independent of the laser irradiation. Impressively, the NP showed negligible toxicity against the HeLa cells in dark, but exhibited its toxicity upon exposure to laser irradiation due to the generation of ROS from the photosensitizer Ce6, which could irreversibly damage the cell membrane.⁴¹ Notably, the cytostatic effects increased with the increase in concentration of Dox or the content of Ce6 under irradiation. Meanwhile, the Dox@NP exhibited the most effective cytotoxicity under the laser irradiation compared with all of the other groups, which was attributed to the light-activated PDT and light-triggered hypoxia chemotherapy. The enhanced cytostatic effects suggested that this living nanocarrier integrated photodynamic therapy and hypoxia responsive chemotherapy has a synergistic effect to suppress the tumor cell growth.

Then, the HeLa tumor-bearing mice were used as tumor xenograft model to evaluate the in vivo tumor-targeted capability via NIR fluorescence imaging. The Dox@NP solution was injected via tail vein administration, as shown in Figure 6a. A remarkable fluorescence signal of Dox was detected at the tumor site after 3 h injection, and the strongest fluorescence signal was observed 6 h after injection. Then, the normal tissues and tumor were collected 24 h after injection to image (Figure 6b) and to analyze the region-of-interest (ROI) (Figure 6c); the data further indicated that Dox@NP had a great potential to accumulate in tumor via the EPR effect.^{12,31,42} However, the remarkable fluorescence signals were mainly observed in liver and kidney when the free Dox solution was administrated via tail vein, as shown in Figures S14 and S15,

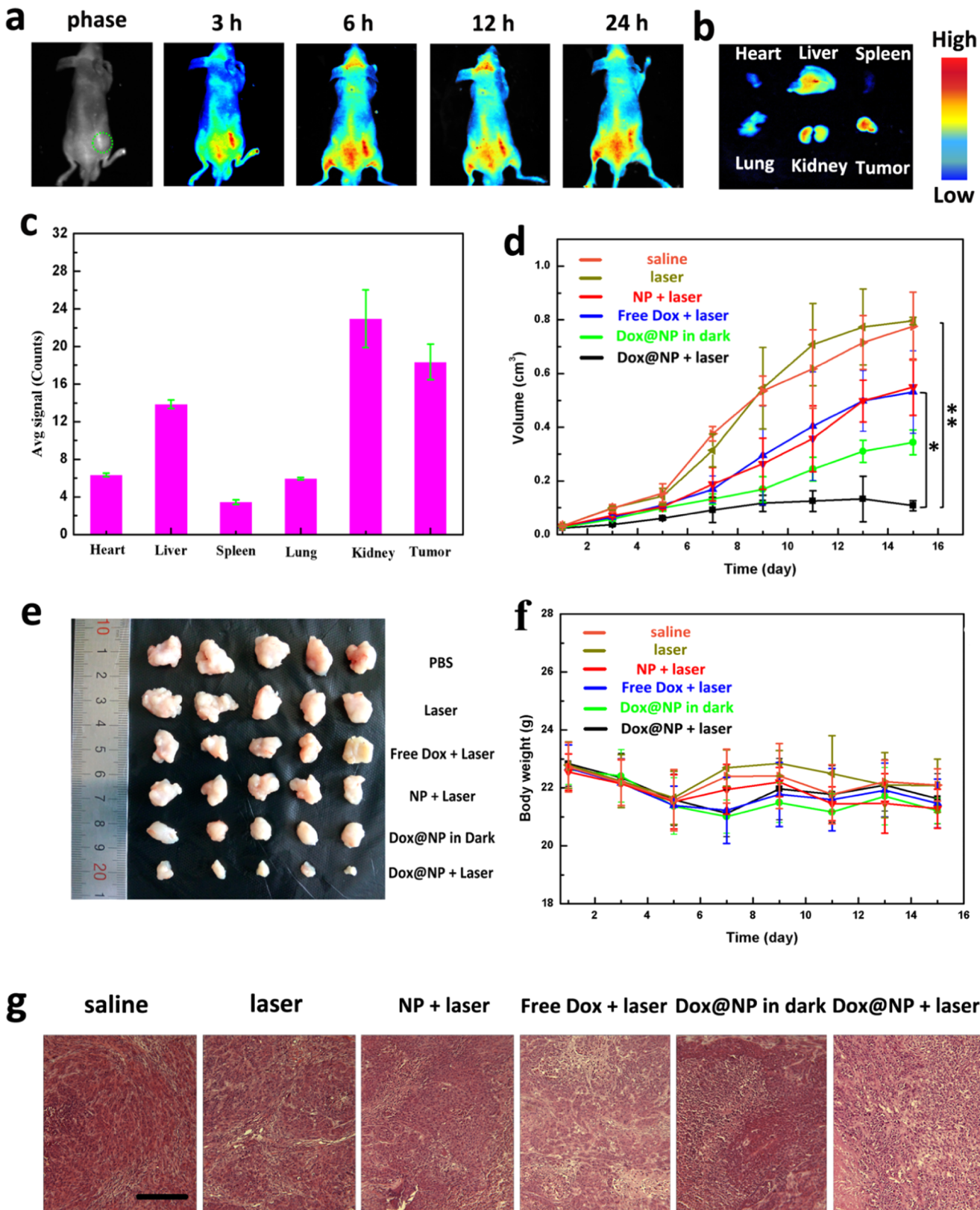


Figure 6. (a) In vivo NIR fluorescence imaging of HeLa tumor bearing nude mice at 3, 6, 12, and 24 h after intravenous injection of Dox@NP. (b) Ex vivo NIR fluorescence imaging of various organs and tumor excised from the mice after injection for 24 h (1: heart, 2: liver, 3: spleen, 4: lung, 5: kidney, 6: tumor). (c) Region-of-interest (ROI) analysis of the fluorescence intensity in tumor and normal organs treated by Dox@NP. (d) Tumor growth curves in HeLa tumor bearing nude mice treated with different samples (1: saline, 2: laser, 3: free Dox with laser irradiation, 4: NP with laser irradiation, 5: Dox@NP in dark, 6: Dox@NP with laser irradiation. Dox: 3 mg/kg, Ce6: 2.3 mg/kg). (e) Representative images of the tumor after different treatments. (f) Relative body weight variation of the mice during the treatment. (g) Hematoxylin and eosin (H&E) analysis of tumor after treatment via Dox@NP with laser irradiation or other formulations. Scale bar: 10 μ m.

and only a small quantity of drug was accumulated in the tumor without the help of the EPR effect, which was in agreement with previous works.^{26,33,43}

In addition, the in vivo anticancer efficacy of Dox@NP was assessed in HeLa tumor-bearing mice. Different formulations were injected via tail vein administration and treated with various methods, including saline, laser, free Dox with laser, NP with laser, and Dox@NP with or without laser. As shown in Figure 6d,e, the free Dox, NP with laser irradiation, and Dox@NP in dark exhibited moderate tumor growth suppression capability due to the monotherapy of chemotherapy or PDT. Impressively, it is remarkable that Dox@NP brought about the greatest efficacy on tumor growth inhibition upon laser irradiation, which was attributed to the light-induced PDT and synchronous hypoxia responsive chemotherapy, indicating a synergistic effect on cancer therapy. It should be noted that no large changes in body weight of mice are observed during the treatment, as shown in Figure 6f. Hematoxylin and eosin (H&E) assays were used to evaluate the anticancer efficacy of various formulations. As shown in Figure 6g, the Dox@NP exhibited remarkable necrosis of tumor cells under the laser irradiation, and negligible damage to normal organs was determined (shown in Figure S16), indicating a high safety of this living drug delivery system.

4. CONCLUSIONS

In conclusion, PDT promoted the formation of hypoxia microenvironment, whereas continuous consumption of oxygen during PDT aggravated the extent of hypoxia. Based on this, a new living drug delivery system integrated the PDT and hypoxia-responsive chemotherapy has been designed and performed, which was made up with three primary constituents: the hypoxia-induced cleaved azobenzene (Azo) bridges, the biodegradable hydrophobic poly(ϵ -caprolactone) (PCL), and photosensitizer chlorine e6 (Ce6)-decorated hydrophilic poly(ethylene glycol) (PEG). Ce6 is an efficient photosensitizer in clinical setting for inducing the oxygen to convert the ROS under the irradiation of light and then resulting in the destruction of tumor cells and blood vessels. Meanwhile, the continuous consumption of oxygen could remarkably facilitate intracellular low-oxygen microenvironment. Further, the hypoxia-responsive diphenylazacarboxylate linker is prepared to reduce stepwise by reductases to aniline derivatives under the oxygen-deficient environment, resulting in the hypoxia-triggered drug release, and providing a synergistic therapy with PDT on the suppression of tumor growth. This new “living” drug delivery system opened a new avenue to design and fabricate smart drug delivery, which can deliver and release drugs according to the specific biological microenvironment in the body.

■ ASSOCIATED CONTENT

Supporting Information

The Supporting Information is available free of charge on the ACS Publications website at DOI: [10.1021/acsami.8b03506](https://doi.org/10.1021/acsami.8b03506).

Synthesis and characterization of the materials; confocal images, GPC tests, hematoxylin and eosin (H&E) analysis, ex vivo NIR fluorescence imaging and region-of-interest (ROI) analysis of the fluorescence intensity ([PDF](#))

■ AUTHOR INFORMATION

Corresponding Authors

*E-mail: xjma@ciac.ac.cn (X.M.).
*E-mail: thy@ciac.ac.cn (H.T.).
*E-mail: xfyu@ciac.ac.cn (X.Y.).

ORCID

Xiaojing Ma: [0000-0001-5073-4748](https://orcid.org/0000-0001-5073-4748)

Huayu Tian: [0000-0002-2482-3744](https://orcid.org/0000-0002-2482-3744)

Xifei Yu: [0000-0003-4654-6941](https://orcid.org/0000-0003-4654-6941)

Author Contributions

[†]W.W. and L.L. contributed equally to this work.

Funding

The financial support from the Nation Natural Science Foundation of China (21674109, 21603214, and 21474104) is acknowledged.

Notes

The authors declare no competing financial interest.

■ REFERENCES

- (1) Dougherty, T. J.; Gomer, C. J.; Henderson, B. W.; Jori, G.; Kessel, D.; Korbelik, M.; Moan, J.; Peng, Q. Photodynamic Therapy. *J. Natl. Cancer Inst.* **1998**, *90*, 889–905.
- (2) Dolmans, D. E.; Fukumura, D.; Jain, R. K. Photodynamic Therapy for Cancer. *Nat. Rev. Cancer* **2003**, *3*, 380–387.
- (3) Idris, N. M.; Gnanasammandhan, M. K.; Zhang, J.; Ho, P. C.; Mahendran, R.; Zhang, Y. In Vivo Photodynamic Therapy Using Upconversion Nanoparticles as Remote-Controlled Nanotransducers. *Nat. Med.* **2012**, *18*, 1580–1590.
- (4) Dai, L.; Yu, Y.; Luo, Z.; Li, M.; Chen, W.; Shen, X.; Chen, F.; Sun, Q.; Zhang, Q.; Gu, H.; Cai, K. Photosensitizer Enhanced Disassembly of Amphiphilic Micelle for ROS-Response Targeted Tumor Therapy in Vivo. *Biomaterials* **2016**, *104*, 1–17.
- (5) Kim, K.; Lee, C. S.; Na, K. Light-Controlled Reactive Oxygen Species (ROS)-Producible Polymeric Micelles with Simultaneous Drug-Release Triggering and Endo/Lysosomal Escape. *Chem. Commun.* **2016**, *52*, 2839–2842.
- (6) Tibbitt, M. W.; Langer, R. Living Biomaterials. *Acc. Chem. Res.* **2017**, *50*, 508–513.
- (7) Qian, C.; Yu, J.; Chen, Y.; Hu, Q.; Xiao, X.; Sun, W.; Wang, C.; Feng, P.; Shen, Q. D.; Gu, Z. Light-Activated Hypoxia-Responsive Nanocarriers for Enhanced Anticancer Therapy. *Adv. Mater.* **2016**, *28*, 3313–3320.
- (8) Perche, F.; Biswas, S.; Wang, T.; Zhu, L.; Torchilin, V. P. Hypoxia-Targeted siRNA Delivery. *Angew. Chem., Int. Ed.* **2014**, *53*, 3362–3366.
- (9) Kulkarni, P.; Haldar, M. K.; You, S.; Choi, Y.; Mallik, S. Hypoxia-Responsive Polymersomes for Drug Delivery to Hypoxic Pancreatic Cancer Cells. *Biomacromolecules* **2016**, *17*, 2507–2513.
- (10) Kang, L.; Fan, B.; Sun, P.; Huang, W.; Jin, M.; Wang, Q.; Gao, Z. An Effective Tumor-Targeting Strategy Utilizing Hypoxia-Sensitive siRNA Delivery System for Improved Anti-Tumor Outcome. *Acta Biomater.* **2016**, *44*, 341–354.
- (11) Blanco, E.; Shen, H.; Ferrari, M. Principles of Nanoparticle Design for Overcoming Biological Barriers to Drug Delivery. *Nat. Biotechnol.* **2015**, *33*, 941–951.
- (12) Pelaz, B.; Alexiou, C.; Alvarez-Puebla, R. A.; Alves, F.; Andrews, A. M.; Ashraf, S.; Balogh, L. P.; Ballerini, L.; Bestetti, A.; Brendel, C.; et al. Diverse Applications of Nanomedicine. *ACS Nano* **2017**, *11*, 2313–2381.
- (13) Wang, Y.; Kohane, D. S. External Triggering and Triggered Targeting Strategies for Drug Delivery. *Nat. Rev. Mater.* **2017**, *2*, No. 17020.
- (14) Hua, H.; Zhu, R.; Sun, W.; Cai, K.; Chen, Y.; Yin, L. Selective Cancer Treatment via Photodynamic Sensitization of Hypoxia-Responsive Drug Delivery. *Nanoscale* **2018**, *10*, 2856–2865.

- (15) Guo, D.; Xu, S.; Wang, N.; Jiang, H.; Huang, Y.; Jin, X.; Xue, B.; Zhang, C.; Zhu, X. Prodrug-embedded angiogenic vessel-targeting nanoparticle: A Positive Feedback Amplifier in Hypoxia-Induced Chemo-Photo Therapy. *Biomaterials* **2017**, *144*, 188–198.
- (16) Vaupel, P.; Schlenger, K.; Knoop, C.; Hockel, M. Oxygenation of Human Tumors-Evaluation of Tissue Oxygen Distribution in Breast Cancers by Computerized O₂ Tension Measurements. *Cancer Res.* **1991**, *51*, 3316–3322.
- (17) Helmlinger, G.; Yuan, F.; Dellian, M.; Jain, R. K. Interstitial pH and pO₂ Gradients in Solid Tumors in Vivo: High-Resolution Measurements Reveal a Lack of Correlation. *Nat. Med.* **1997**, *3*, 177–182.
- (18) Liao, D.; Johnson, R. S. Hypoxia: A Key Regulator of Angiogenesis in Cancer. *Cancer Metastasis Rev.* **2007**, *26*, 281–290.
- (19) Vaupel, P.; Mayer, A. Hypoxia in Cancer: Significance and Impact on Clinical Outcome. *Cancer Metastasis Rev.* **2007**, *26*, 225–239.
- (20) Zheng, X.; Wang, X.; Mao, H.; Wu, W.; Liu, B.; Jiang, X. Hypoxia-Specific Ultrasensitive Detection of Tumours and Cancer Cells in Vivo. *Nat. Commun.* **2015**, *6*, No. 5834.
- (21) Qian, C.; Feng, P.; Yu, J.; Chen, Y.; Hu, Q.; Sun, W.; Xiao, X.; Hu, X.; Bellotti, A.; Shen, Q.-D.; Gu, Z. Anaerobe-Inspired Anticancer Nanovesicles. *Angew. Chem., Int. Ed.* **2017**, *56*, 2588–2593.
- (22) Wang, Y.; Xie, Y.; Li, J.; Peng, Z.-H.; Sheinin, Y.; Zhou, J.; Oupicky, D. Tumor-Penetrating Nanoparticles for Enhanced Anticancer Activity of Combined Photodynamic and Hypoxia-Activated Therapy. *ACS Nano* **2017**, *11*, 2227–2238.
- (23) Fingar, V. H.; Henderson, B. W. Drug and Light Dose Dependence of Photodynamic Therapy—a Study of Tumor and Normal Tissue-Response. *Photochem. Photobiol.* **1987**, *46*, 837–841.
- (24) Henderson, B. W.; Fingar, V. H. Relation of Tumor Hypoxia and Response to Photodynamic Treatment in an Experimental Mouse-Tumor. *Cancer Res.* **1987**, *47*, 3110–3114.
- (25) Mitchell, J. B.; McPherson, S.; Degraff, W.; Gamson, J.; Zabell, A.; Russo, A. Oxygen Dependence of Hematoporphyrin Derivative-Induced Photoinactivation of Chinese-Hamster Cells. *Cancer Res.* **1985**, *45*, 2008–2011.
- (26) Duan, X.; Xiao, J.; Yin, Q.; Zhang, Z.; Yu, H.; Mao, S.; Li, Y. Smart pH-Sensitive and Temporal-Controlled Polymeric Micelles for Effective Combination Therapy of Doxorubicin and Disulfiram. *ACS Nano* **2013**, *7*, 5858–5869.
- (27) Wang, W.; Wang, B.; Ma, X.; Liu, S.; Shang, X.; Yu, X. Tailor-Made pH-Responsive Poly(choline phosphate) Prodrug as a Drug Delivery System for Rapid Cellular Internalization. *Biomacromolecules* **2016**, *17*, 2223–2232.
- (28) Wang, W.; Wang, B.; Liu, S.; Shang, X.; Yan, X.; Liu, Z.; Ma, X.; Yu, X. Bioreducible Polymer Nanocarrier Based on Multivalent Choline Phosphate for Enhanced Cellular Uptake and Intracellular Delivery of Doxorubicin. *ACS Appl. Mater. Interfaces* **2017**, *9*, 15986–15994.
- (29) Wang, W.; Ma, X.; Yu, X. pH-Responsive Polymersome Based on PMCP-b-PDPA as a Drug Delivery System to Enhance Cellular Internalization and Intracellular Drug Release. *Chin. J. Polym. Sci.* **2017**, *35*, 1352–1362.
- (30) Mura, S.; Nicolas, J.; Couvreur, P. Stimuli-Responsive Nanocarriers for Drug Delivery. *Nat. Mater.* **2013**, *12*, 991–1003.
- (31) Peer, D.; Karp, J. M.; Hong, S.; FaroKhzad, O. C.; Margalit, R.; Langer, R. Nanocarriers as an Emerging Platform for Cancer Therapy. *Nat. Nanotechnol.* **2007**, *2*, 751–760.
- (32) Gao, M.; Hu, A.; Sun, X.; Wang, C.; Dong, Z.; Feng, L.; Liu, Z. Photosensitizer Decorated Red Blood Cells as an Ultrasensitive Light-Responsive Drug Delivery System. *ACS Appl. Mater. Interfaces* **2017**, *9*, 5855–5863.
- (33) Zhang, Y.; Huang, F.; Ren, C.; Yang, L.; Liu, J.; Cheng, Z.; Chu, L.; Liu, J. Targeted Chemo-Photodynamic Combination Platform Based on the DOX Prodrug Nanoparticles for Enhanced Cancer Therapy. *ACS Appl. Mater. Interfaces* **2017**, *9*, 13016–13028.
- (34) Kiyose, K.; Hanaoka, K.; Oushiki, D.; Nakamura, T.; Kajimura, M.; Suematsu, M.; Nishimatsu, H.; Yamane, T.; Terai, T.; Hirata, Y.; Nagano, T. Hypoxia-Sensitive Fluorescent Probes for in Vivo Real-Time Fluorescence Imaging of Acute Ischemia. *J. Am. Chem. Soc.* **2010**, *132*, 15846–15848.
- (35) Kiyose, K.; Tomomi, N.; Mayumi, K.; Makoto, S.; Hiroaki, N.; Hirata, Y.; Nagano, T. Development of Hypoxia-sensitive Fluorescent Probes for Real-time Ischemia Imaging in vivo. *Nitric Oxide* **2010**, *22*, S31–S32.
- (36) Yuan, Y.; Liu, J.; Liu, B. Conjugated-Polyelectrolyte-Based Polyprodrug: Targeted and Image-Guided Photodynamic and Chemotherapy with On-Demand Drug Release upon Irradiation with a Single Light Source. *Angew. Chem., Int. Ed.* **2014**, *53*, 7163–7168.
- (37) Zhao, Z.; Han, Y.; Lin, C.; Hu, D.; Wang, F.; Chen, X.; Chen, Z.; Zheng, N. Multifunctional Core-Shell Upconverting Nanoparticles for Imaging and Photodynamic Therapy of Liver Cancer Cells. *Chem. - Asian J.* **2012**, *7*, 830–837.
- (38) Zhen, X.; Zhang, C.; Xie, C.; Miao, Q.; Lim, K. L.; Pu, K. Intraparticle Energy Level Alignment of Semiconducting Polymer Nanoparticles to Amplify Chemiluminescence for Ultrasensitive In Vivo Imaging of Reactive Oxygen Species. *ACS Nano* **2016**, *10*, 6400–6409.
- (39) Jung, H. J.; Min, H.; Yu, H.; Lee, T. G.; Chung, T. D. Electrochemical Cleavage of Azo Linkage for Site-Selective Immobilization and Cell Patterning. *Chem. Commun.* **2010**, *46*, 3863–3865.
- (40) Guo, X.; Shi, C.; Yang, G.; Wang, J.; Cai, Z.; Zhou, S. Dual-Responsive Polymer Micelles for Target-Cell-Specific Anticancer Drug Delivery. *Chem. Mater.* **2014**, *26*, 4405–4418.
- (41) Høgset, A.; Prasmikaite, L.; Selbo, P. K.; Hellum, M.; Engesaeter, B. O.; Bonsted, A.; Berg, K. Photochemical Internalisation in Drug and Gene Delivery. *Adv. Drug Delivery Rev.* **2004**, *56*, 95–115.
- (42) Pearson, R. M.; Sen, S.; Hsu, H. J.; Pasko, M.; Gaske, M.; Kral, P.; Hong, S. Tuning the Selectivity of Dendron Micelles Through Variations of the Poly(ethylene glycol) Corona. *ACS Nano* **2016**, *10*, 6905–6914.
- (43) Lee, Y.; Kim, H.; Kang, S.; Lee, J.; Park, J.; Jon, S. Bilirubin Nanoparticles as a Nanomedicine for Anti-inflammation Therapy. *Angew. Chem., Int. Ed.* **2016**, *55*, 7460–7463.